Kinetic Analyses Combining Quantum Chemical and Quantum Statistical Methods: Some Case Studies†

Minh Tho Nguyen,* Debasis Sengupta, and Luc G. Vanquickenborne

Department of Chemistry, University of Leuven, Celestijnenlaan 200F, B-3001-Leuven, Belgium

Received: September 20, 1995; In Final Form: January 3, 1996⊗

In this article we present a theoretical approach to the kinetic analyses of chemical reactions by combining quantum chemical calculations with a quantum statistical treatment of rate constants. We first briefly outline the quantum Rice−Ramsperger−Kassel (QRRK) model and describe the ab initio molecular orbital methods employed. We then discuss a sampling of the studies recently carried out in the Laboratory of Quantum Chemistry, University of Leuven. We focus on some prototypical reactions of atmospheric interest including $CH_3 + NO$, $SiH_3 + NO$, $H + HNCO$, and $SiH_2 + C_2H_2(C_2D_2)$. All these reactions are multichannel processes with competing pathways. The good performance of the QRRK treatment in calculating apparent rate constants and thus extracting finer details about reaction mechanisms is demonstrated by comparison with available experimental data. Overall, the observed performance and the less tedious computing work compared to rigorous RRKM methods promote a general use of the QRRK treatment coupled with reliable ab initio calculations in kinetic analysis.

Introduction

Many chemical processes such as the addition of radicals to multiple bonds, oxidation of nitrogen-containing compounds or hydrocarbons, and reactions in photochemistry, in combustion, and in the atmosphere involve complex chain reactions where highly energized species are produced. It is often very difficult to measure their kinetic parameters in laboratory conditions. In order to obtain detailed mechanisms and kinetic parameters of such complex multichannel reactions from kinetic data, the rate constants of various pathways as a function of temperature and pressure need to be simulated via reliable theoretical methods. When possible, such simulations can provide valuable information and finer details regarding the reaction mechanism.

Kineticists are primarily concerned with the evaluation of the rate constants using methods in which activation energies are generally estimated from thermochemical data and vibrational frequencies are often fitted to reproduce the experimental data. Even though the heats of reaction involving new stable species can be obtained from available thermochemical data with a reasonable accuracy, the activation barriers as well as vibrational frequencies and structures of the transition state are difficult to evaluate. As a consequence, kinetic calculations based on less accurate data may lead to erroneous conclusions regarding the reaction mechanism. With the advent of high-speed computers and sophisticated quantum chemical methods, it is now possible to calculate more accurate potential energy surfaces (PES) of such complex multichannel reactions. Vibrational wavenumbers and rotational constants can also be derived with reasonable accuracy. However, up to now, quantum chemists have mainly been interested in the construction of PES. Since a multichannel reaction involves several isomerization steps, it is not always meaningful to predict their feasibility by considering them simply as a juxtaposition of elementary single-step reactions. Clearly, it will be more useful to carry out actual calculations of the rate constants as function of temperature and pressure. Apparently, the complexity and difficulty of the kinetic analysis have often prevented quantum chemists from taking this final step. The need for a simplified but reliable approach is thus obvious. We wish to advocate, by presenting in this paper some of our recent results, the use of a quantum statistical Rice−Ramsperger−Kassel theory (QRRK)[1] coupled with the idea of chemical activation process[2] and based on reliable PES to calculate the rate constants of all reaction pathways as functions of temperature and pressure. The relevant PES have been calculated by means of high-level ab initio molecular orbital calculations. We consider the following multichannel reactions: (i) $SiH_2 + C_2H_2$ (C_2D_2), (ii) $CH_3 + NO$, (iii) $SiH_3 + NO$, and (iv) $H + HNCO$.

SCHEME 1

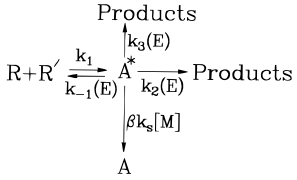

SCHEME 2

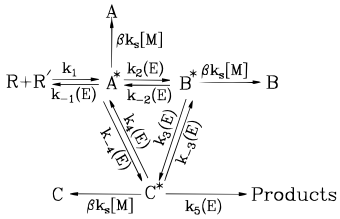

Brief Summary of the QRRK Theory[1]

The initial step of an addition or recombination reaction is usually the formation of an energized complex. Several possible reaction schemes can be written on the basis of the number of reaction and isomerization paths available to the energized complex. For the present purpose we consider different possibilities as displayed in Schemes 1, 2, and 3. The energized complex, A* (superscript ∗ represents a chemically activated complex), arises from a chemical reaction of R and R′, and it can undergo isomerization to give several other energized

† This paper was originally submitted for the S. F. Boys/I. Shavitt Issue [*J. Phys. Chem.* **1996**, *100* (15)].

⊗ Abstract published in *Advance ACS Abstracts,* June 1, 1996.

S0022-3654(95)02778-X CCC: $12.00

SCHEME 3

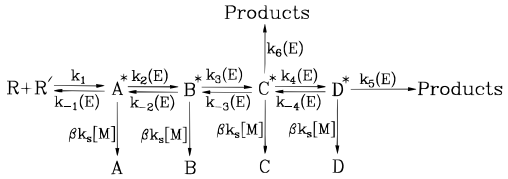

complexes. An energized complex formed in these conditions can produce a nonequilibrium situation where the molecules can acquire energy far in excess of the thermal collisional energy and the complex can undergo several reactions which are otherwise not possible. Hence, these reactions need to be treated in the framework of a chemical activation process.[2] The reactions of the types presented in Schemes 1, 2, and 3 involve the competition between stabilization and dissociation of the complexes and should not be treated as elementary single-step reactions. In other words, the overall (apparent) rate constants are more meaningful than the rate constants for the individual steps.

Now it is straightforward to evaluate the apparent rate constant for the formation of the stabilized and reaction products. For example, the rate constant for the stabilized product, A, from the reactants in the Scheme 2, is given by

$$K_{sA} = \frac{1}{[R][R']}\sum_{E_{crit}}^{\infty}\beta k_s[M][A^*]f(E) \qquad (1)$$

Similarly, the apparent rate constant for the product formation can be expressed as

$$K_{rxn} = \frac{1}{[R][R']}\sum_{E_{crit}}^{\infty}k_5(E)[C^*]f(E) \qquad (2)$$

where [A*] and [C*] are the steady state concentrations of A* and C*, $f(E)$ is the chemical activation distribution function, and E_{crit} is the activation energy for the dissociation to the reactants. The steady state concentrations of the energized adduct can be readily evaluated in terms of the energy dependent rate constants, $k_i(E)$. The apparent rate constants and the chemical activation distribution function can be evaluated by calculating the rate constants of individual processes $[k_i(E)]$ based on either Rice−Ramsperger−Kassel (RRK)[3] or Rice−Ramsperger−Kassel−Marcus (RRKM)[4] theory. In RRKM theory, the steady state concentration of an activated complex is considered during the formation of the products from the energized molecule. A rotational−vibrational density of states term for the activated complex thus appears in the expression of $k_i(E)$. Hence, the summation should be replaced by an integration in the case of RRKM theory. In contrast, the RRK theory takes into account the energy distribution among the vibrational modes in the molecule. Even though the energy dependencies of $k_i(E)$ are best treated by the RRKM theory, there is no doubt that the major contribution is due to vibrational energies.[5] The major advantage of the RRK theory is a substantial simplification in the practical calculation. Indeed, the smaller amount of input data required makes the treatment much less tedious. Moreover, recent reports on the calculation of the rate constants via RRK theory for several reactions show reasonably good agreement with experimental data.[1,6] For further details about QRRK theory, we refer to the paper by Dean.[1] The values of the collisional stabilization rate constant are computed using Lennard-Jones collision rate theory.[7] The collision efficiency, β, can be calculated as[8]

$$\beta/(1-\beta^{1/2}) = -\langle\Delta E\rangle/F_E k_b T \qquad (3)$$

where $-\langle\Delta E\rangle$ is the average energy transferred per collision, F_E is a factor which reflects the energy dependence of the density of states, and k_b and T are the Boltzman constant and temperature, respectively. Equation 3 holds nearly exactly when $-\langle\Delta E\rangle$ is much less than the thermal energy of the system. In most cases, the value of F_E has been taken as 1.15.[9] For very high temperatures, the following expression has been used to evaluate β:[10]

$$\beta = \frac{\langle E\rangle_d/(\langle E\rangle_d + F_E k_b T)}{\int_0^{E_0} N(E)\left[1 - \frac{F_E k_b T}{\langle E\rangle_d + F_E k_b T}\exp\left(-\frac{E_0 - E}{F_E k_b T}\right)\right]} \qquad (4)$$

where $\langle E\rangle_d$ is the average energy transferred per collision in the down transition, E_0 is the threshold energy for the dissociation of the complex, and $N(E)$ is the normalized Boltzmann distribution function.[10] The denominator of the above equation has been calculated by a numerical method, and the Whitten−Rabinovitch approximation[11] was used to calculate $N(E)$ and F_E. It should be noted that only vibrational degrees of freedom were included in the calculation of the density of states. In the present case $-\langle\Delta E\rangle$ and $\langle E\rangle_d$ were assumed to be independent of temperature.

The frequency factors are evaluated as

$$A_F = \frac{k_b T}{h}\frac{Q\#}{Q} \qquad (5)$$

where $Q\#$ and Q are the complete partition functions of the transition state and reactants, respectively. In cases where there is no transition state, the frequency factors were taken from the literature, and we found they are thermodynamically consistent.

To calculate the total rate constant we have adopted the following procedure. The total rate constant for the disappearance of the reactants (K'_T) is given by the relation (see, for example, Scheme 1)

$$K'_T[R][R'] = [K_{rxn,A} + K_{stab,A} + K_{back}][R][R']$$

or

$$[K'_T - K_{back}][R][R'] = [K_{rxn,A} + K_{stab,A}][R][R'] \qquad (6)$$

where K_{back}, $K_{rxn,A}$, and $K_{stab,A}$ are the rate constants for back reaction, product formation from A, and stabilization of the energized adduct A, respectively. Here we have assumed that the back reaction is one of the channels which is responsible for the disappearance of the reactants. Since the back reaction leads to products which are nothing but the reactants, the experimentally measured total rate constant (K_T) can be calculated as

$$K_T = K'_T - K_{back}$$
$$= K_{rxn,A} + K_{stab,A} \qquad (7)$$

In general, the total (apparent) rate constant is the sum of the rate constants of all the product channels originating from the reactants.

Quantum Chemical Methods

All ab initio quantum chemical calculations were performed using the GAUSSIAN 92 program package.[12] Initial geometry optimizations for the reactions considered were carried at the

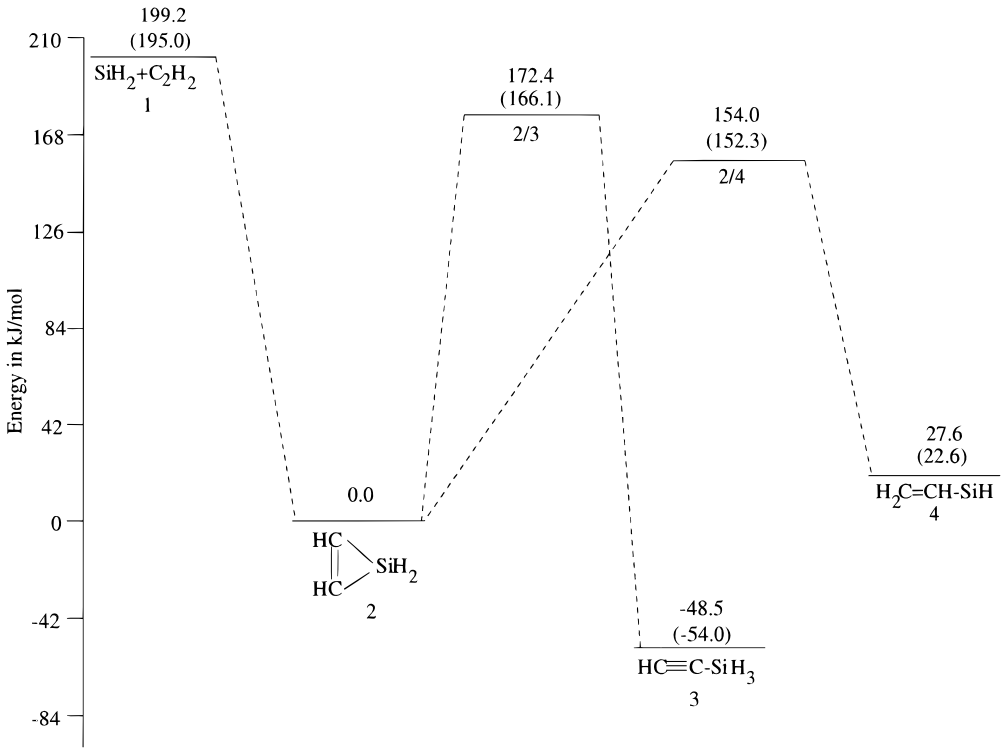

Figure 1. Schematic potential energy profile showing the $SiH_2 + C_2H_2$ addition and the rearrangements of the silylene adduct. Relative energies obtained from QCISD(TC)/6-311G++(2df,2p)+ZPE and QCISD(T)/6-311++G(d,p)+ZPE (within parentheses) calculations.

Hartree−Fock level with the dp-polarized 6-31G(d,p) basis set. The identity of each transition state structure has been determined, when necessary, by intrinsic reaction coordinate (IRC) calculations. The geometrical parameters of the relevant stationary points were then reoptimized at the second-order perturbation theory level, MP2/6-31G(d,p). Vibrational wavenumbers were calculated using 6-31G(d,p) basis sets with either the HF or MP2 method. Single-point energy calculations, using the quadratic configuration interaction methods, QCISD(T)/6-311++G(d.p) and QCISD/6-311++G(2df,2p), were subsequently performed on all relevant stationary points for the reactions i and ii using optimized MP2 geometries. For reaction iii, similar calculations were performed only at the QCISD(T)/6-311++G(d,p) level. For reaction iv we performed single-point energy calculations at the QCISD(T)/6-311++G(d,p) and QCISD/6-311++G(2df,2pd) levels using MP2/6-31G(d,p) optimized geometries. Vibrational wavenumbers calculated at the HF and MP2 levels are scaled down by a factor of 0.90 and 0.95, respectively. Contributions due to the triple excitations were calculated from the following relation:

$$E(\text{QCISD(TC)/L}) = E(\text{QCISD/L}) + E(\text{QCISD(T)/S}) - E(\text{QCISD/S}) \quad (8)$$

where L and S refer to the relatively larger and smaller basis sets, respectively, and E(QCISD(TC)) refers to the energy corrected for triple excitations. The above relation essentially assumes that the energy correction for triple excitations is the same for both smaller and larger basis sets.

Applications

In the following section we apply the QRRK theory[1] as briefly outlined above for four multichannel reactions i, ii, iii, and iv. The main objective of our study is to analyze the mechanism of these complex reactions rather than just reproducing the experimental results.

(i) Reaction of SiH_2 and C_2H_2(C_2D_2). Silylene is recognized as an important intermediate in the pyrolysis of silanes; it is also known to play a key role in the modern methods for preparing thin films of amorphous silicon.[13] Owing to its importance in organosilicon chemistry, a large number of experimental and theoretical reports have appeared in the literature on the stability and the chemical reactivity of this species. Chou et al.[14] reported the experimental evaluation of absolute rate constants for silylene addition to several hydrocarbons. Very recently, Becerra and Walsh[15] reported an extensive experimental study of the silylene addition reaction to acetylene and deuterated acetylene (C_2D_2) over the temperature range 291−613 K in the presence of SF_6 as bath gas. This reaction was found to be pressure dependent, suggesting a third-body-assisted association reaction. Moreover, the reaction with C_2D_2 was found to be faster than that with C_2H_2. The following reaction pathways were suggested (eq 9).[15]

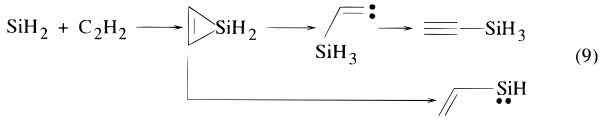

(9)

The same authors also calculated the rate constants using the RRKM method where the activation barriers were estimated from thermochemical data and the transition state structures were constructed by adjusting vibrational frequencies to match the entropy of activation; the reaction was not treated via chemical activation processes. We have first explored the PES obtained by MO calculations of various possible channels of the $SiH_2 + C_2H_2$ reaction. A schematic diagram of the PES is shown in Figure 1. Becerra and Walsh[15] suggested that **2** rearranges to **3** via the intermediate silylvinylidene (see eq 9). However, we were not able to locate any equilibrium structure corresponding to **5**. Therefore, we believe that silylvinylidene does not exist as a discrete species. To calculate the apparent rate constants we consider Scheme 4, which is similar to Scheme 1.

SCHEME 4

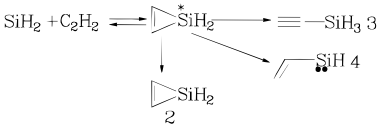

TABLE 1: Comparison of the Rate Constants (cm^3 mol^{-1} s^{-1}) Related to the $SiH_2 + C_2H_2$ Reaction Using Energetics from Two Different Levels of ab Initio Calculations at 500 K and 10 Torr Pressure

rate constants	QCISD(TC)/ 6-311++G(2df,2p)	QCISD(T)/ 6-311++G(d,p)
K_2	1.527×10^{12}	1.265×10^{12}
K_3	8.896×10^{11}	9.821×10^{11}
K_4	1.226×10^{13}	7.788×10^{12}
K_{2D}	3.316×10^{12}	2.780×10^{12}
K_{3D}	7.428×10^{11}	8.931×10^{11}
K_{4D}	1.619×10^{13}	1.061×10^{13}
K_T	1.469×10^{13}	1.003×10^{13}
K_{TD}	2.005×10^{13}	1.429×10^{13}

The apparent rate constants of the various pathways for the reaction of $SiH_2 + C_2H_2$ and $SiH_2 + C_2D_2$ (SiH_2 is in its singlet ground state) are defined as

$$SiH_2 + C_2H_2 \rightarrow \mathbf{2}\ (K_2)$$

$$SiH_2 + C_2H_2 \rightarrow \mathbf{3}\ (\text{via } \mathbf{2}^*)\ (K_3)$$

$$SiH_2 + C_2H_2 \rightarrow \mathbf{4}\ (\text{via } \mathbf{2}^*)\ (K_4)$$

$$SiH_2 + C_2D_2 \rightarrow \mathbf{2D}\ (K_{2D})$$

$$SiH_2 + C_2D_2 \rightarrow \mathbf{3D}\ (\text{via } \mathbf{2D}^*)\ (K_{3D})$$

$$SiH_2 + C_2D_2 \rightarrow \mathbf{4D}\ (\text{via } \mathbf{2D}^*)\ (K_{4D})$$

where D stands for the reaction with deuterated acetylene. Since the above reactions are concurrent, the total rate constant for the disappearance of the reactants (K_T and K_{TD}) can be calculated as[16]

$$K_T = K_2 + K_3 + K_4$$

and

$$K_{TD} = K_{2D} + K_{3D} + K_{4D}$$

The QRRK calculations have been carried out with SF_6 as bath gas. The value of $-\langle\Delta E\rangle$ ($-\langle\Delta E\rangle = 7.1$ kJ/mol) has been taken from ref 8. The values of A_1 and A_{-1} have been taken as 6.16×10^{13} cm^3 mol^{-1} s^{-1} and 6.03×10^{16} s^{-1}, respectively.[15] In a recent paper,[17] we have calculated these rate constants using energies obtained by QCISD(TC)/6-311++G(2df,2p). For the purpose of comparison and as a calibration for future studies on larger systems, we have recalculated rate constants using a lower level of sophistication, namely, QCISD(T)/6-311++G-(d,p) (Figure 1). As seen in Table 1, the values of the rate constants using results from two different levels of accuracy are almost the same, and their variations with temperature and pressure remain similar. This is probably due to the large energy release during the formation of **2** from **1**, which is much higher than the activation barrier for formation of **3** and **4**. Figure 2a shows the variation of K_T as a function of total pressure at two different temperatures. It can be seen that the falloff region shifts toward higher pressure with increasing temperature. This is the well-known behavior of the stabilization rate constants. Thus, K_T attains a value of 6.02×10^{13} cm^3 mol^{-1} s^{-1} at the high-pressure limit. These results are in reasonable agreement with the available experimental observations, i.e., $\sim 10^{14}$ cm^3 mol^{-1} s^{-1}.[15] Figure 2b shows the plot of log K_T and log K_{TD} as a function of temperature at two different pressures, e.g., 0.132 atm (~100 Torr) and higher pressure. The rate constant for the disappearance of the reactants (Figure 2b) increases with decrease in temperature (negative temperature effect). This observation is again in agreement with the experimental result.[15] While the rate constant for the reaction of SiH_2 with C_2H_2 is lower than that with C_2D_2 at low pressure (see curves A and B

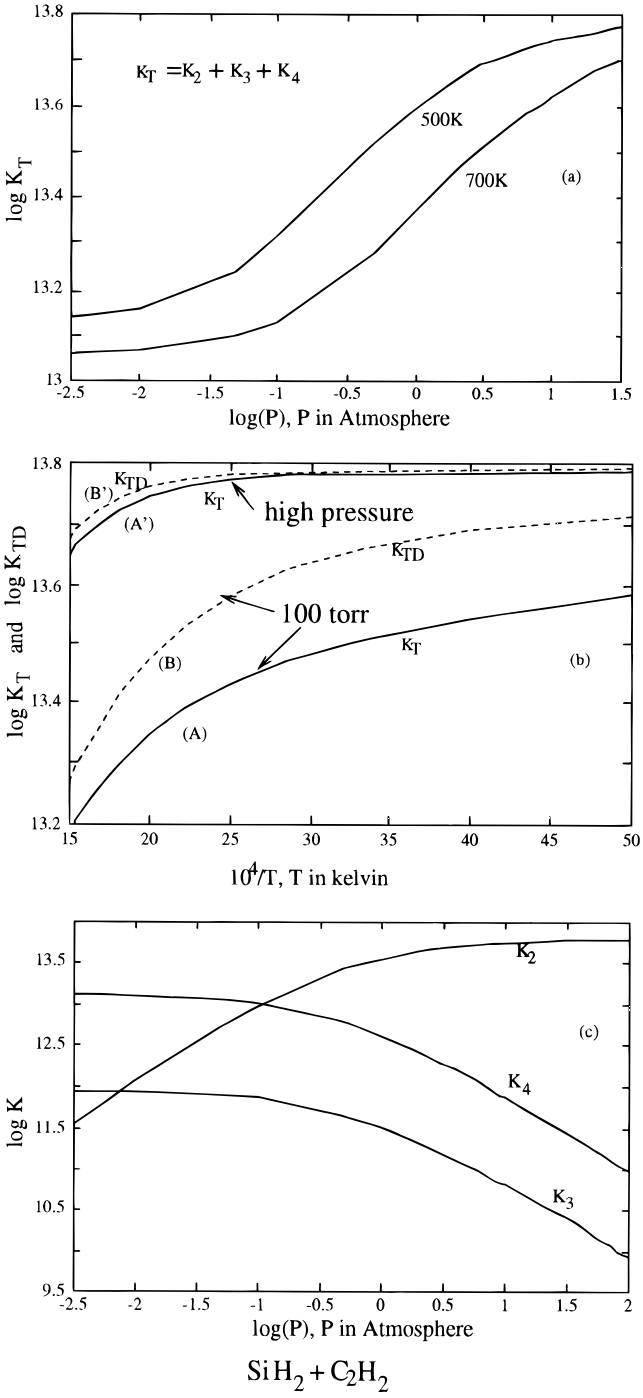

Figure 2. (a) Variation of total rate constant K_T with total pressure at two different temperatures. SF_6 has been taken as bath gas. (b) Variation, with temperature, of the total rate constants, K_T and K_{TD}, at two different pressures. Curves A and B refer to 0.132 atm (100 Torr), while curves A′ and B′ refer to the high-pressure limit, i.e., 10 atm. (c) Variation, with pressure, of various apparent rate constants for the formation of **2**, **3**, and **4** at 500 K.

in Figure 2b), at the high-pressure limit both were found to be nearly the same (see curves A′ and B′ in Figure 2b). Our calculated rate constants, K_T and K_{TD}, at the high-pressure limit vary from 6.11×10^{13} to 4.23×10^{13} cm^3 mol^{-1} s^{-1} in the temperature range 200−700 K. By comparison, the experimental values vary from 2.4×10^{14} to 1.2×10^{14} cm^3 mol^{-1} s^{-1}.[15] Even though our calculated rate constants are 3−4 times smaller than the experimental values, it gives the correct trend. Figure 2c shows the variation of the apparent rate constants of all possible channels presented in Figure 1 as a function of the total pressure at 500 K. It can be seen that while the formation of **3** and **4** decreases, the formation of **2** increases with increasing pressure. A comparison of parts a and c of Figure 2 reveals that the disappearance of the reactants in the lower pressure region is primarily due to the formation of **4**, while at higher pressure the reactants disappear due to formation of **2**. Hence, the pressure dependence of K_T is due to the formation of **2** via the stabilization of the energized adduct.

Figure 3a,b,c displays the variation of all the apparent rate constants of the $SiH_2 + C_2H_2$ reaction with temperature at three different pressures. At low pressure (Figure 3a) the kinetics is primarily dominated by the formation of **2** and **4** in the lower temperature region. At higher temperatures, the **1** → **4** channel opens up and becomes the primary source for the disappearance of the reactants. Channel **1** → **3** remains unimportant at all temperatures. As the pressure increases (Figure 3b), the **1** → **2** channel dominates over the **1** → **4** channel until the temperature reaches 500 K. Above 500 K the variation of K_T is primarily due the formation of **4** and **2**. The variation of all the apparent rate constants at the high-pressure limit is illustrated in Figure 3c. It reveals that K_T (or K_{TD}) is dominated by the formation of **2**. K_2 (or K_{2D}) always remains higher than K_3 (or K_{3D}) and K_4 (or K_{4D}) at all temperatures. K_2 and K_{2D} are also nearly identical and show a slight negative temperature dependence. Examination of Figures 2a and 3b suggests that the negative temperature effect of K_T (or K_{TD}) at low pressure is due the combined effect of K_2 and K_3 (or K_{2D} and K_{3D}). At the high-pressure limit this is due to the negative temperature dependence of K_2 (or K_{2D}).

(ii) Reaction of CH_3 and NO. Nitric oxide radical, NO, is well-known as one of the most toxic pollutants. NO also plays an important role in the stratospheric ozone depletion and in the formation of acid rain. During the combustion of hydrocarbons, several radicals are produced which can react with NO and break the N═O bond. One such reaction is $CH_3 + NO$. Even though several experimental reports have appeared on the kinetic aspects of the $CH_3 + NO$ reaction,[18] identification of the products has been reported only recently.[19,20] Lifshitz et al.[19] found that the primary product channel for the $CH_3 + NO$ reaction is the formation of $HCN + H_2O$. They suggested that this reaction occurs via the 1,2 hydrogen shift of CH_3NO, which is the rate-determining step. Saito et al.[21] studied the thermal decomposition of formaldoxime, $H_2C{=}N{-}OH$, where $HCN + H_2O$ were found to be the products. This suggests that a possible mechanism for the formation of HCN and H_2O in the $CH_3 + NO$ reaction could be the following:

$$CH_3 + NO \rightarrow CH_3NO\ (\mathbf{6}) \rightarrow H_2C{=}NHO\ (\mathbf{7}) \rightarrow H_2C{=}N{-}OH\ (\mathbf{8}) \rightarrow HCN + H_2O \quad (10)$$

Several temperature dependence studies suggest that the bimolecular rate constant for the disappearance of the reactants is in the range $\sim 10^9 - 10^{10}$ cm^3 mol^{-1} s^{-1} at 1500 K with a total density of $\sim 10^{-6}$ mol/cm^3.[18] Pilling and co-workers[22] also studied the pressure dependence of the total rate constant at lower temperatures.

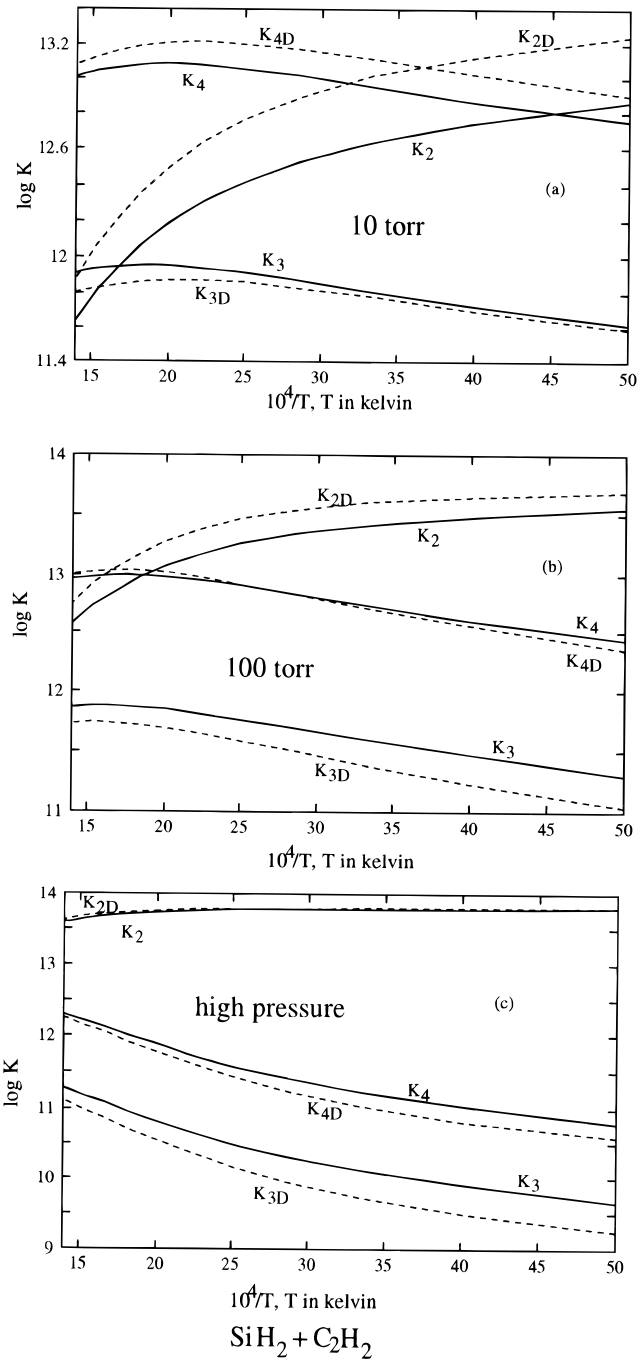

Figure 3. Variation, with temperature, of the apparent rate constant for the formation of **2**, **3**, and **4** at (a) 10 Torr, (b) 100 Torr, and (c) high pressure (10 atm).

We have explored the PES corresponding to the reactions in eq 10 by means of ab initio MO calculations, as mentioned earlier. The schematic representation of the PES is shown in Figure 4, where different routes for the formation of the final products are shown. Direct formation of **8** from **6** via TS **6**/**8** for 1,3 hydrogen shift has a relatively large activation energy compared to that via TS **6**/**7** for 1,2 hydrogen shift. These results are in agreement with the earlier ab initio calculation by Adeney et al. using a lower level of theory.[23] Similarly, indirect formation of the final products **10** from **8** via TS **8**/**9** has a considerably lower barrier than that of the direct process, namely, via TS **8**/**10**. To calculate the rate constants of the several pathways as a function of temperature and pressure via QRRK theory, we consider Scheme 5, which is similar to Scheme 2.

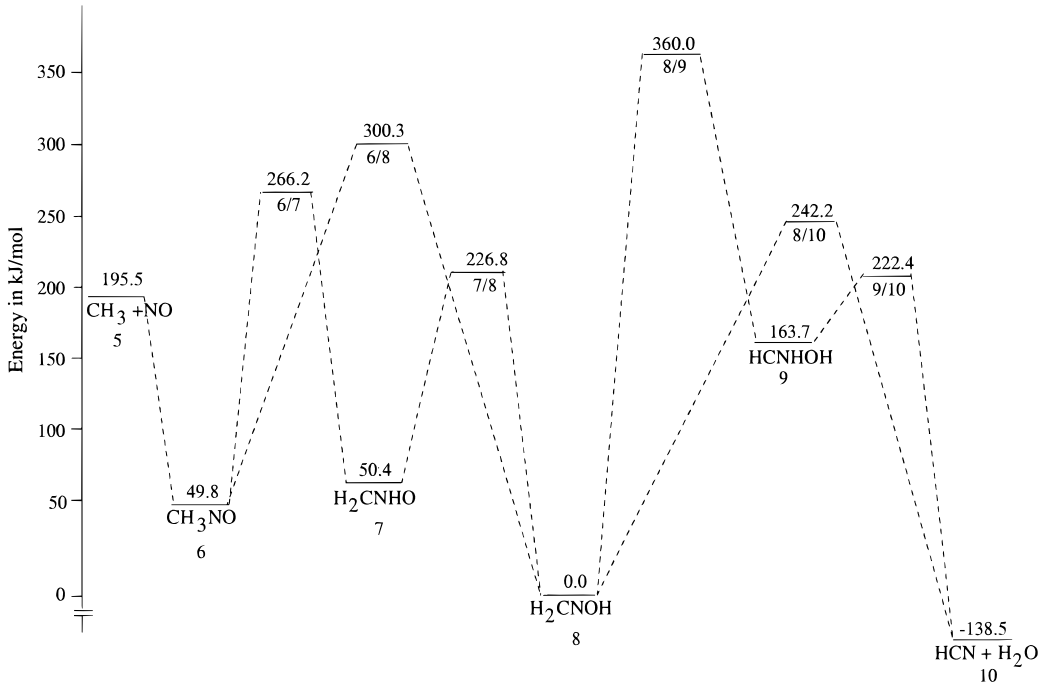

Figure 4. Schematic potential energy profile showing the CH_3 + NO reaction. Relative energies are obtained from QCISD(TC)/6-311G++(2df,2p)+ZPE calculations.

SCHEME 5

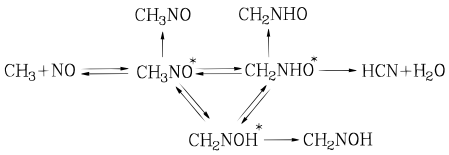

It should be noted that formation of the products from **8** via carbene **9** has been eliminated from Scheme 5 because of its very high activation barrier. Frequency factors for CH_3 + NO → CH_3NO and its reverse process were calculated to be 1.01 × 10^{13} cm^3 mol^{-1} s^{-1} and 3.20 × 10^{14} s^{-1} using the data obtained by Kaiser[24] and Lifshitz et al.[19] In the QRRK calculation, argon has been taken as bath gas. The value of $-\langle\Delta E\rangle$ for argon ($-\langle\Delta E\rangle$ = 2.63 kJ/mol) has been taken from ref 8. The collision efficiency, β, has been calculated from eq 3. The values of β change from 0.363 to 0.079 as the temperature increases from 300 to 2500 K.

The apparent rate constants for the various processes are defined as

$$CH_3 + NO \rightarrow CH_3NO\ (K_6)$$

$$CH_3 + NO \rightarrow H_2CNHO\ (K_7)$$

$$CH_3 + NO \rightarrow H_2CNOH\ (K_8)$$

$$CH_3 + NO \rightarrow H_2O + HCN\ (K_{10})$$

The total rate constant K_T for the CH_3 + NO reaction is given by

$$K_T = K_6 + K_7 + K_8 + K_{10}$$

Figure 5 shows the variation of K_6 and K_{10} with respect to pressure at two different temperatures, 300 and 1100 K. It shows that the falloff curve shifts toward the higher pressure region with increasing temperature. Formation of the products is very low at lower temperatures. This is due to the higher activation energies for the processes occurring from CH_3NO. With the increase in temperature, there is, as expected, a large increase in the rate constant for the product formation. Figure 5 also shows that there is no appreciable variation of K_{10} with pressure, but at very high pressure K_{10} actually decreases due to the very strong stabilization of CH_3NO*. The value of the stabilization rate constant of CH_3NO*, K_6, at 296 K and a pressure of 0.795 atm (or 604 Torr) is calculated to be 7.4 × 10^{12} cm^3 mol^{-1} s^{-1}. This value compares well with the experimental value of 4.11 × 10^{12} cm^3 mol^{-1} s^{-1} at similar conditions.[22] Figure 6 shows the variation with temperature of all apparent rate constants between 900 and 2500 K at a total density of 10^{-6} mol/cm^3. At the lower temperature region, the disappearance of the reactants is primarily due to the formation of stabilized CH_3NO. As the temperature increases, the channel for the product formation (HCN + H_2O) becomes more important. At 1850 K it takes over the rate of formation of CH_3NO and becomes the primary channel for the disappearance of the reactants. The formation of H_2C═NHO and H_2C═NOH is not very significant as far as the disappearance of the reactants

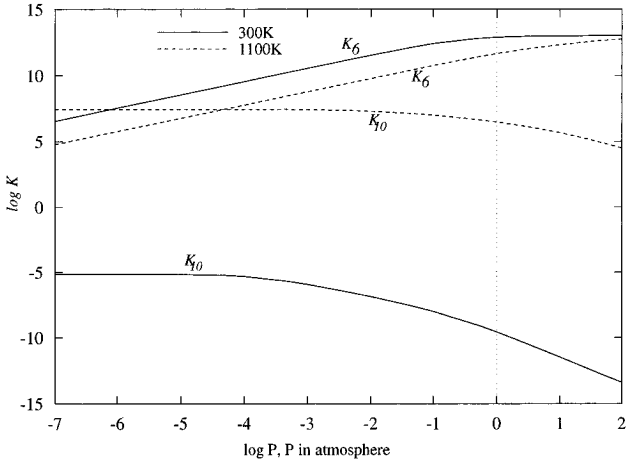

Figure 5. Variation of the apparent rate constants with respect to pressure for the formation of stabilized CH_3NO (K_6) and HCN + H_2O (K_{10}) at two different temperatures.

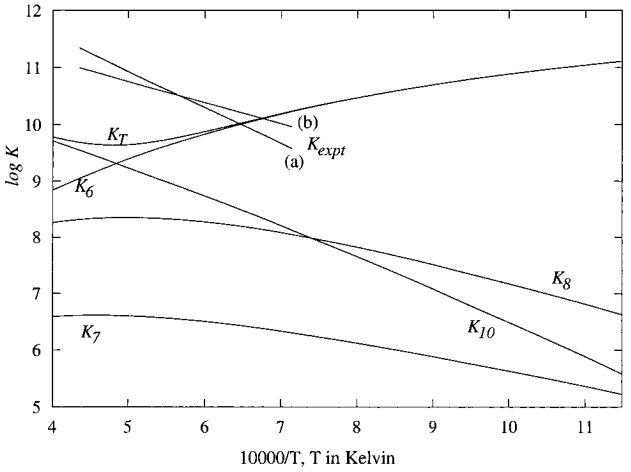

Figure 6. Variation, with temperature, of the apparent rate constants of all the channels for the CH_3 + NO reaction at a total density of 10^{-6} cm^3/mol. Experimental rate constants (K_{expt}) are also shown: (a) from ref 18a and (b) from ref 20.

is concerned. The calculated total rate constant (Figure 6) was found to be 1.19×10^{10} cm^3 mol^{-1} s^{-1} at 1500 K, which is in good agreement around 1500 K. For example, at 1500 K the calculated values of 1.19×10^{10} cm^3 mol^{-1} s^{-1} compares well with the available experimental results ($\sim 10^9 - 10^{10}$ cm^3 mol^{-1} s^{-1}).[18,22] At higher temperatures, however, the experimental values are approximately 1 order of magnitude higher than our calculated values. This indicates that the mechanism of this reaction may be more complex and needs further theoretical investigation. The rate constant for the formation of the final products HCN + H_2O (K_{10}) was found to be 1.0×10^8 cm^3 mol^{-1} s^{-1} at 1300 K. We find that this value is 1 order of magnitude lower than that of the experimental rate constant.[19]

As we discussed earlier, formation of **8** from **6** can be realized either via the intermediate **7** (1,2 hydrogen shift) or via direct 1,3 hydrogen shift. Since the formation of the final products depends on the steady state concentration of **8***, it will be interesting to examine how the two different pathways contribute to the formation of the final products. The ratio of the formation of **8** via two different routes at unit concentration of the reactants can be written as

$$R = \sum_{E_{crit}}^{\infty} \frac{k_3(E)[CH_2NHO^*]}{k_{-4}(E)[CH_3NO^*]} f(E) \qquad (11)$$

Our calculations show that R varies from 297 to 4 as the temperature increases from 900 to 2500 K. This clearly indicates that formation of final products via direct 1,3 hydrogen shift in CH_3NO is not important in the lower temperature region, but at very high temperatures, the 1,3 shift of hydrogen might contribute appreciably.

(iii) Reaction of SiH_3 and NO. Although the silyl radical, SiH_3, is known to play a major role in the combustion of silanes and in the chemical vapor deposition process, its reactions have not been investigated very extensively. Krasnoparov and co-workers[25] studied the reactions of SiH_3 with S_2Cl_2, O_2, and ClNO. Slage et al.[26] measured the reaction rates with O_2 and N_2O in the temperature range 296−500 K. Recently, Sugwara et al.[26] measured the rate constants of SiH_3 reactions with O_2, NO_2, and NO. Their pressure dependence studies showed that the SiH_3 + NO reaction is a third-body-assisted association reaction, but, so far, no report on the temperature dependence study of this reaction seems to be available. In this section, we, therefore, theoretically calculate the rate constant for the various reaction channels as functions of temperature and pressure in an effort to predict the reaction mechanism. Figure 7 shows the PES surface of the SiH_3 + NO reaction which is, in many aspects, analogous to the CH_3 + NO reaction. It should be noted that we were unable to locate the transition structure TS **12**/**14** for 1,3 hydrogen shift of SiH_3NO at the MP2 level of theory. Hence, to obtain an idea about a possible position of TS **12**/**14**, we performed a single-point calculation at the QCISD(T)/6-311++G(d,p) level on the HF/6-31G(d,p) optimized transition structure. Calculation shows that it lies more than 50 kJ/mol above TS **12**/**13**. It will be a reasonable approximation to eliminate the **12** → **14** transformation via direct 1,3 hydrogen shift. The data in Figure 7 clearly show that the activation barrier for direct H_2O loss from the oxime, **14**, is higher than that of silylene, **15**, formation, in contrast to the similar processes in CH_3 + NO at the same level of calculations. The difference arises primarily from the fact that while H_2CNOH, **8**, is more stable than carbene **9**, H_2SiNOH, **14**, is actually less stable than silylene, **15**. For the calculation of the rate constants via QRRK theory, we consider Scheme 6, which is similar to Scheme 3.

As an approximation, the frequency factors for SiH_3 + NO → SiH_3NO and its reverse process have been taken to be the same as those in the CH_3 + NO reaction. N_2 is taken as bath gas and its $-\langle\Delta E\rangle$ ($-\langle\Delta E\rangle$ = 3.47 kJ/mol) value is obtained from ref 8. The apparent rate constants for several pathways are defined as

$$SiH_3 + NO \rightarrow \mathbf{12}\ (K_{12})$$

$$SiH_3 + NO \rightarrow \mathbf{13}\ (K_{13})$$

$$SiH_3 + NO \rightarrow \mathbf{14}\ (K_{14})$$

$$SiH_3 + NO \rightarrow \mathbf{15}\ (K_{15})$$

$$SiH_3 + NO \rightarrow \mathbf{16}\ (\text{directly from } \mathbf{14})\ (K_{16}^{14})$$

$$SiH_3 + NO \rightarrow \mathbf{16}\ (\text{from } \mathbf{15})\ (K_{16}^{15})$$

Figure 8 summarizes the variation of K_{12}, K_{16}^{14}, and K_{16}^{15} as a function of total pressure at two different temperatures. As in the CH_3 + NO reaction, the falloff region shifts toward the higher pressure region with increasing temperature. K_{16}^{15} and K_{16}^{14} remain invariant until the pressure reaches 1 atm. At higher pressures, both K_{16}^{14} and K_{16}^{15} decrease sharply. This observation is again similar to that of CH_3 + NO. It should be noted that β varies from 0.422 to 0.099 as the temperature increases from 300 to 2500 K. The bimolecular rate constant for SiH_3 + NO reaction at 300 K and 0.0132 atm (10 Torr) is calculated to be 6.1×10^{11} cm^3 mol^{-1} s^{-1}, which compares reasonably with the experimental value of 2.5×10^{12} cm^3 mol^{-1} s^{-1}.[27] Figure 9 displays the variation with temperature of all apparent rate constants at 0.0132 atm (10 Torr) pressure. Formation of **12** thus remains the primary channel for the disappearance of the reactants to 1800 K. Above 1800 K, the formation of the final products, HSiN + H_2O, becomes the main channel. K_{13}, K_{14}, and K_{15} remain unimportant at all temperatures. Hence, we predict that if the reaction is carried out at temperatures above 1800 K, there might be a possibility of HSiN and H_2O formation. Figure 9 also shows that K_{16}^{15} is always larger than K_{16}^{14}, clearly indicating that formation of the final products via the direct **14** → **16** pathway has a much lower probability than that via the indirect pathway, i.e., **14** → **15** → **16**. This is no doubt due to the larger activation barrier for **14**

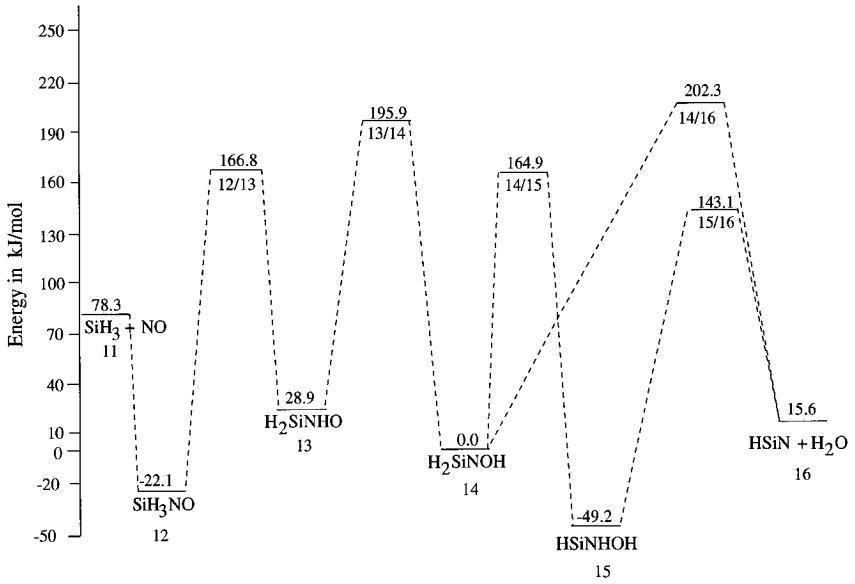

Figure 7. Schematic potential energy profile showing the SiH_3 + NO reaction. Relative energies are obtained from QCISD(T)/6-311G++(d,p)+ZPE calculations.

SCHEME 6

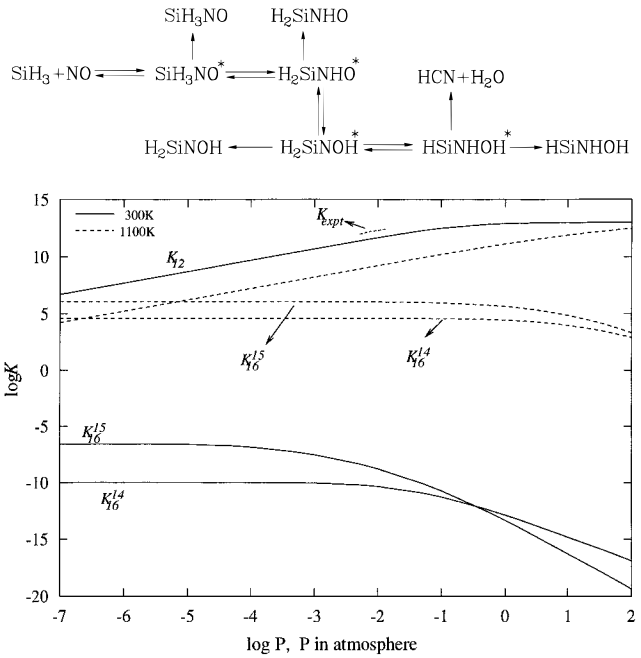

Figure 8. Variation of the apparent rate constant with respect to pressure for the formation of stabilized SiH_3NO (K_{12}) and HCN + H_2O via two different routes, i.e., **14** → **16** (K_{16}^{14}) and **14** → **15** → **16**) (K_{16}^{15}), at two different temperatures. K_{expt} values are obtained from ref 27.

→ **15** than that for the **14** → **16** transformation. Agreement between experimental observation and our theoretical calculation confirms that the formation of adduct, SiH_3NO, is the only product channel in the lower temperature region. The quantity R is defined as

$$R = \sum_{E_{crit}}^{\infty} \frac{k_5(E)[\mathrm{HSiNHOH^*}]}{k_6(E)[\mathrm{H_2SiNOH^*}]} f(E)$$

which is a measure of formation of the final products via two different routes, namely, **14** → **15** → **16** and **14** → **16**. The value of R varies between 27 and 5 as the temperature is increased from 300 to 2500 K. This indicates that formation

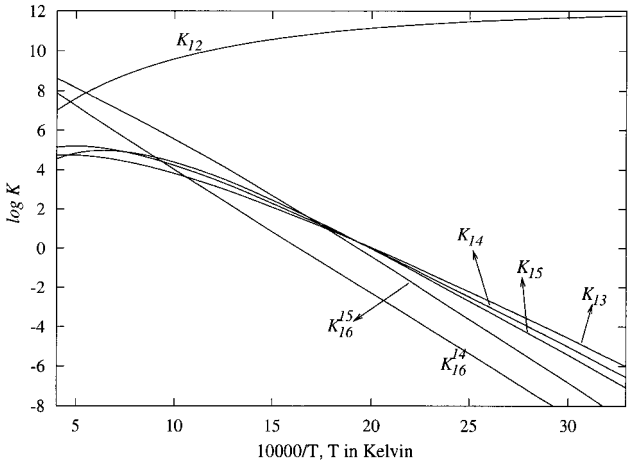

Figure 9. Variation, with temperature, of all the channels for the SiH3 + NO reaction at a total pressure of 1.32×10^{-2} atm (or 10 Torr).

of the final products (HSiN + H_2O) from H_2SiNOH, **14**, occurs through a multistep pathway at lower temperatures, but at very high temperatures, product formation might also take place via a direct mechanism from **14**.

At this stage, it is interesting to emphasize the difference in the mechanism of product formation of two analogous reactions, SiH_3 + NO and CH_3 + NO. For this purpose, we have calculated the PES for CH_3 + NO at the QCISD(T)/6-311++G-(d,p) level of theory. The conclusions of the kinetic analysis as discussed in the preceding section, however, remain unchanged. Even though both reactions produce similar kinds of products, their detailed mechanisms are completely different. While the formation of HCN + H_2O from H_2C═NOH (**8**) occurs via a direct mechanism, an indirect mechanism via the formation of silylene, **15**, is preferred for the formation of HSiN + H_2O and thereby HNSi, which is the more stable isomer.

(iv) Reactions of H and HNCO. The development of effective after-treatment processes aimed at the removal of nitric oxide from combustion products continues to attract considerable interest. In the RAPRENOX process proposed by Perry and Siebers,[28] isocyanic acid, which is formed following thermal decomposition of the injected cyanuric acid, has been assumed to play an important role as an initiator and precursor of NH_2, an NO-reducing agent (eqs a-d). While (a) and (b) constitute

the initiation steps, (c) is presumably the key step of the entire process.

$$HNCO \rightarrow HN + CO \text{ (a)}$$

$$HN + NO \rightarrow H + N_2O \text{ (b)}$$

$$H + HNCO \rightarrow H_2N + CO \text{ (c)}$$

$$H_2N + NO \rightarrow HN_2 + OH \text{ (d)}$$

Mertens and co-workers[29] studied the kinetics of the H + HNCO reaction in a shock-heated mixture of HNCO diluted in argon; they measured the second-order rate coefficient over a temperature range 2340−3270 K, attributing the process to the formation of H_2N + CO. In a subsequent theoretical study, Miller and Melius[30] considered both channel c and e of the H + HNCO reaction.

$$H + HNCO \rightarrow H_2 + NCO \text{ (e)}$$

$$NCO + H_2 \rightarrow HNCO + H \text{ (f)}$$

These authors[30] calculated the rate coefficients of both reactions c and d using BAC-MP4/6-31G(d,p) energies (bond additive correction fourth-order perturbation theory) in conjunction with UHF/6-31G(d,p) geometries and vibrational wavenumbers. They found that (c) is the dominant product channel over a wide range of temperature (300−3300 K) and that it involves the H_2NCO intermediate, whose formation constitutes the rate-determining step. Nevertheless, the kinetic analysis has been carried out by Miller and Melius[30] with some adjustment to the vibrational wavenumbers in order to obtain a qualitative agreement with experiment. In fact, the out-of-plane bending wavenumber of the transition structure for addition obtained by Hartree−Fock calculations has been found to be too low and has been replaced by that estimated at the second-order perturbation (MP2) calculation.

In principle, isocyanic acid exhibits four distinct reaction centers susceptible to attack by the hydrogen atom. The reactions c and e arise from the addition of hydrogen atom to N of HNCO and abstraction of H from HNCO, respectively. To the best of our knowledge, the C- and O-additions have not been investigated yet. It is thus important to assess the influence of other product channels on the NH_2 formation, in order to ascertain the predominance of channel c. On the other hand, the rate constant for the reverse reaction involving the NCO radical (reaction f) has also been measured in shock tube[31] and excimer laser photolysis[32] experiments.

The purpose of the present study is to re-examine the H + HNCO reaction system by considering the attack of H at the four possible sites of HNCO. In addition, the rate constants for the reaction c, e, and f have been calculated with the help of QRRK theory. We also examine the effect on the rate constants of replacing hydrogen by deuterium (i.e., D + DNCO).

Our ab initio MO calculations at the PUMP4/6-311++G-(d,p)//MP2/6-31G(d,p)+ZPE level of theory demonstrate that the addition of hydrogen to the nitrogen center of HNCO has the lowest activation barrier, followed by hydrogen abstraction.

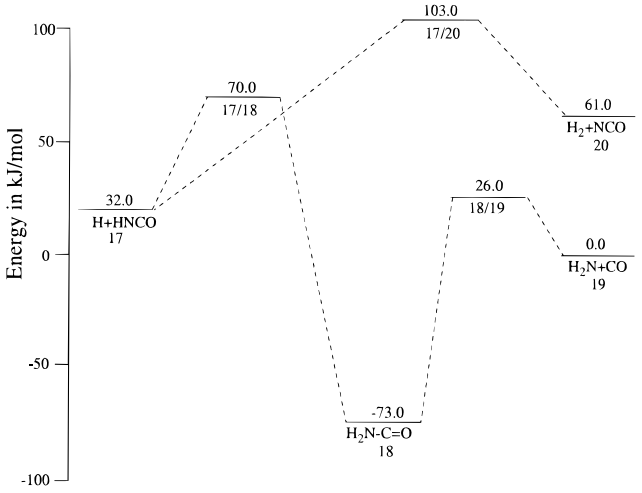

Figure 10. Schematic potential energy profile showing H-abstraction and N-addition using QCISD(TC)/6-311++G(2df,2pd)+ZPE.

SCHEME 7

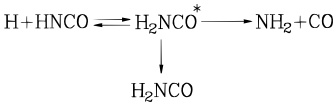

Thus, the attack of the hydrogen atom on the carbon and oxygen centers of HNCO is an unfavorable process. To obtain an improved PES for the addition of H to N in HNCO and also for the hydrogen abstraction, we further performed calculations at the QCISD(TC)/6-311++G(2df,2pd) level, as discussed in a previous section, for these two processes, whose schematic representation of the PES is illustrated in Figure 10.

To calculate the rate constant for the reaction using QRRK theory, we consider Scheme 7, which is very similar to Scheme 1 except that there is only one reaction channel.

The rate constant for the hydrogen abstraction process has been calculated using the classical equation

$$k = A_F \exp\left(-\frac{E_0}{k_b T}\right) \quad (12)$$

The role of tunneling during hydrogen transfer reactions, especially in the low-temperature region, is well established.[33] Since both reactions under investigation involve the transfer of hydrogen, it is essential to include a tunneling correction for the rate constants. The symmetric Eckart potential[34] is often used[35] to include the contribution of hydrogen tunneling to the rate constant. The symmetric Eckart potential is given by[34]

$$V(x) = \frac{V^*}{\cosh^2[x\sqrt{(F^*/2V^*)}]} \quad (13)$$

where x is the reaction coordinate, V^* is the activation barrier, and F^* is the curvature at the potential energy maximum.

The Schroedinger equation for the Eckart potential can be solved, and for an incident particle of mass μ and energy E, the tunneling probability is given by[34]

$$K(\zeta) = \frac{\cosh(2\alpha\sqrt{\zeta}) - 1}{\cosh(2\alpha\sqrt{\zeta}) + \cosh\sqrt{4\alpha^2 - \pi^2}} \quad (14)$$

where $\zeta = E/V^*$ and $\alpha = 2\pi V^*/h\nu^*$; ν^* is the absolute value of the imaginary frequency at the saddle point. The tunneling correction (q_c), which is the ratio of the quantum mechanically calculated rate constant to that calculated classically, is given

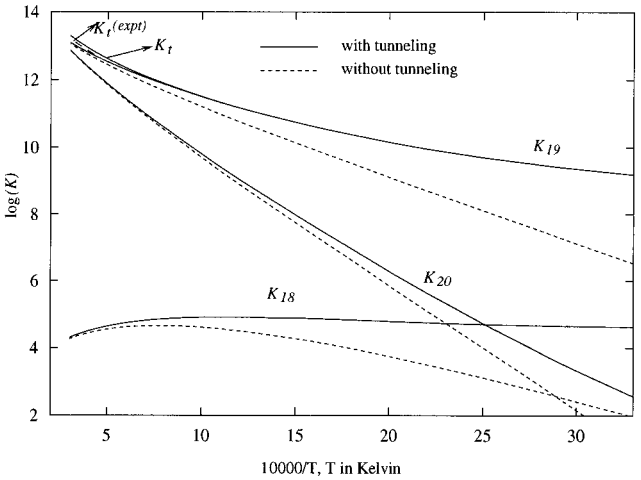

Figure 11. Variation, with temperature, of the rate constants for all the reaction pathways arising from the H + HNCO reaction. Experimental plots taken from ref 28 are also shown (see text for definitions).

by the following equation:[33]

$$q_c = \exp\left(\frac{E_0}{k_b T}\right) \int_0^\infty \frac{1}{k_b T} K(\zeta) \exp\left(\frac{-E}{k_b T}\right) dE \qquad (15)$$

The integration in eq 15 was solved by a numerical method.

In the present case, the tunneling correction, q_c, has been multiplied with the rate constants for the processes H + HNCO → NH_2CO and H + HNCO → H_2 + NCO to include the effect of tunneling.

We define the rate constants as

$$H + HNCO \rightarrow NH_2CO\ (K_{18})$$

$$H + HNCO \rightarrow NH_2 + CO\ (\text{via } H_2NCO^*)\ (K_{19})$$

$$H + HNCO \rightarrow H_2 + NCO\ (K_{20})$$

$$H_2 + NCO \rightarrow H + HNCO\ (\text{reaction } f)\ (K_f)$$

The total rate constant (K_t) for the disappearance of the reactants (i.e., H and HNCO) can be written as

$$K_t = K_{18} + K_{19} + K_{20}$$

Since the QRRK calculations have been performed in the very high temperature region, the calculation of the collision efficiency, β, has been carried out using eq 4. For the rate constant of stabilization, argon has been considered as bath gas. The value of $-\langle\Delta E\rangle$ ($-\langle\Delta E\rangle$ = 3.47 kJ/mol) is obtained from ref 8. The values of β, calculated from eq 4, change from 6.9 × 10^{-5} to 3.4 × 10^{-6} as the temperature increases from 300 to 3300 K. The variation of K_{18}, K_{19}, and K_{20} with temperature at atmospheric pressure as shown in Figure 11 reveals that tunneling is important in the lower temperature region. At higher temperatures, the tunneling corrections for all reactions approach unity. The rate constants for the formation of H_2 + NCO is much lower than that of NH_2 + CO at lower temperatures. Formation of the stabilized adduct, NH_2CO, remains unimportant almost over the entire temperature range studied here (300−3300 K). Under these conditions, it could be quite difficult to detect NH_2CO experimentally even though it is the most stable species. At higher temperatures, both K_{19} and K_{20} attain nearly the same value. For example, at 3300 K, K_{19} = 1.2 × 10^{13} cm^3 mol^{-1} s^{-1} and K_{20} = 7.5 × 10^{12} cm^3 mol^{-1} s^{-1}. Experimental values of the total rate constant (K_t) for H + HNCO are available only in the temperature range 2340−3270 K.[29] For comparison, the experimental values of

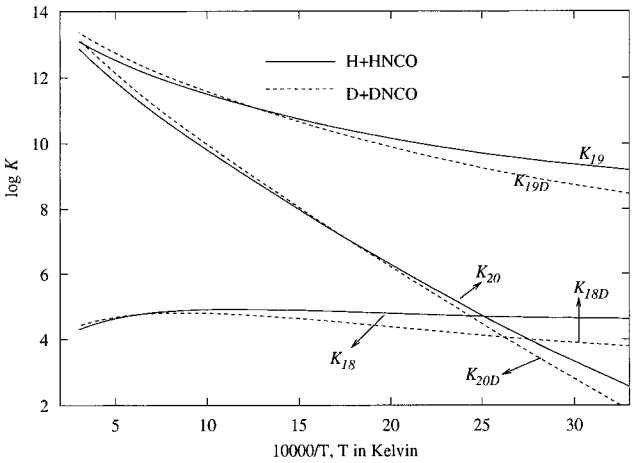

Figure 12. Comparison of all apparent rate constant for the reactions H + HNCO and D + DNCO.

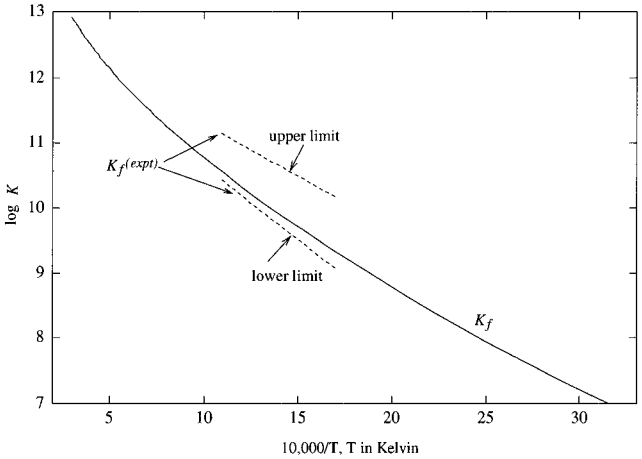

Figure 13. Variation, with temperature, of the rate constant for the H_2 + NCO reaction. Experimental results shown are taken from ref 32.

K_t are also plotted in Figure 11. It can be seen that our calculated values are in excellent agreement with the available experimental results.[29] For example, at 3200 K, our calculated value of K_t is 1.82 × 10^{13} cm^3 mol^{-1} s^{-1}, while the corresponding experimental value is 1.47 × 10^{13} cm^3 mol^{-1} s^{-1}. The rate constants K_{19} and K_{20} vary between 1.47 × 10^9 to 1.24 × 10^{13} cm^3 mol^{-1} s^{-1} and 3.0 × 10^2 to 7.48 × 10^{12} cm^3 mol^{-1} s^{-1}, respectively, in the temperature range 300−3300 K. Figure 11 also indicates that the rate constant for the disappearance of the reactants (K_t) is primarily due to the formation of the H_2N + CO channel. To calculate the isotope effect on the rate constant, we recalculated vibrational frequencies, rotational constants, and zero-point energies of all the stationary points by replacing the hydrogens by deuterium. Figure 12 compares the various rate constants for the H + HNCO and D + DNCO reactions. K_{18D}, K_{19D}, and K_{20D} (subscript D represents the corresponding rate constants for the D + DNCO reaction) are consistently smaller than the corresponding rate constants for the H + HNCO reaction at lower temperatures. At higher temperatures the rate constants for the D + DNCO reaction turn out to be larger than for the H + HNCO reaction.

To our knowledge, there are no experimental data available for K_{20}, but there are two experimental reports[31,32] on the kinetic study for the reverse reaction, NCO + H_2 → H + HNCO. To compare the results of our calculations with experiment, we also calculated the rate constant for the reaction NCO + H_2 → H + HNCO (reaction f mentioned above), following eq 12. Figure 13 shows the variation of the calculated values of K_f as a

function of temperature and compares with experimental values within the available temperature range (i.e., 592−913 K and 1490 K). The calculated values for K_f fall well within the uncertainty of the experimental results.

Concluding Remarks

The potential energy surfaces of four multichannel reactions which are of importance in atmospheric chemistry have been calculated using high-level ab initio molecular orbital methods. Subsequently, the QRRK theory together with the idea of the chemical activation process has been applied to calculate the rate constants of available reaction channels. Results of the calculations show good agreement with experimental results. Several interesting features regarding the reaction mechanisms have been discussed which could not be obtained in experiment. We wish to suggest that it is necessary to explore PES followed by kinetic analyses to establish the reaction mechanism of such complex multichannel reactions where chemically activated species are formed as intermediates. For this purpose, the QRRK approach coupled with energetic results obtained from, for example, the QCISD(T)/6-311++G(d,p) level appears to be a good choice for a rapid but reliable analysis of complex kinetics.

Acknowledgment. The authors thank Professor Jozef Peeters from our department for valuable discussion and the reviewers for their valuable suggestions. We are also indebted to the Belgian Science organizations (NFWO, DWTC, GOA) for continuing support.

References and Notes

(1) Dean, A. M. *J. Phys. Chem*. **1985**, *89*, 4600.
(2) Robinson, P. J.; Holbrook, K. A. Unimolecular Reactions; Wiley-Interscience: 1972; Chapter 8.
(3) Chapter 4 of ref 2.
(4) Chapter 3 of ref 2.
(5) Chapter 1 of ref 2.
(6) Bozzelli, J. W.; Dean, A. M. *J. Phys. Chem*. **1989**, *93*, 1058; **1993**, *97*, 4427.
(7) Troe, J. *J. Chem. Phys*. **1977**, *66*, 4758.
(8) Gardiner, W. C.; Troe, J. *Combustion Chemistry*; Gardiner, W. C., Ed.; Springer-Verlag: New York, 1984; p 173.
(9) Troe, J. *J. Chem. Phys*. **1979**, *83*, 114.
(10) Gilbert, R. G.; Luther, K.; Troe, J. *Ber. Bunsen-Ges. Phys. Chem*. **1983**, *98*, 169.
(11) Whitten, G. Z.; Rabinovitch, B. S. *J. Chem. Phys*. **1963**, *38*, 2466; **1964**, *41*, 1883.
(12) Frisch, M. J.; Trucks, G. W.; Schlegel, H. B.; Gill, P. M. W.; Johnson, B. G.; Wong, M. W.; Foresman, J. B.; Robb, M. A.; Head-Gordon, M.; Replogle, E. S.; Gomperts, R.; Andres, J. L.; Raghavachari, K.; Binkley, J. S.; Gonzalez, C.; Martin, R. L.; Fox, D. J.; DeFrees, D. J.; Baker, J.; Stewart, J. J. P.; Pople, J. A. *Gaussian 92/DFT*, Revision, F.4; Gaussian, Inc.: Pittsburgh, PA, 1993.
(13) Jasinski, J. M.; Meyerson, B. S.; Scott, B. A. *Annu. Rev. Phys. Chem*. **1987**, *38*, 109.
(14) Chou, J. O.; Beach, D. B.; Jasinski, J. M. *J. Phys. Chem*. **1987**, *91*, 5340.
(15) Becerra, R.; Walsh, R. *Int. J. Chem. Kinet*. **1994**, *26*, 45.
(16) Benson, S. W. Thermochemical Kinetics; John Wiley & Sons.: Inc.: New York, 1976; Chapter 1.
(17) Nguyen, M. T.; Sengupta, D.; Vanquickenborne, L. G. *Chem. Phys. Lett*. **1995**, *240*, 513.
(18) Yang, H.; Lissianski, V.; Okoroanyanwu, J. U.; Gardiner, W. C.; Shin, K. S. *J. Phys. Chem*. **1993**, *90*, 10042. (b) Hoffmann, A.; Wagner, H. Gg.; Wolff, Th.; Hwang, S. M. *Ber. Bunsen-Ges. Phys. Chem*. **1990**, *94*, 1407. (c) Wolff, Th.; Wagner, H. Gg. *Ibid*. **1988**, *92*, 678. (d) Pilling, M. J.; Robertson, J. A.; Rogers, G. J. *Int. J. Chem. Kinet*. **1976**, *VIII*, 883. (e) Baldwin, A. C.; Golden, D. M. *Chem. Phys. Lett*. **1978**, *55*, 350.
(19) Lifshitz, A.; Tamburu, C.; Frank, P.; Just, T. *J. Phys. Chem*. **1993**, *97*, 4085.
(20) Hennig, G.; Wagner, H. Gg. *Ber. Bunsen-Ges. Phys. Chem.* **1994**, *98*, 749.
(21) Saito, K.; Makishita, K.; Kakumoto, T.; Sasaki, T.; Imamura, A. *J. Phys. Chem*. **1988**, *92*, 4371.
(22) Davies, J. W.; Green, N. J. B.; Pilling, M. J. *J. Chem. Soc., Faraday Trans*. **1991**, *87*, 2317.
(23) Adeney, P. D.; Bouma, W. J.; Radom, L.; Rodwell, W. R. *J. Am. Chem. Soc*. **1980**, *102*, 4069.
(24) Kaiser, E. W. *J. Phys. Chem*. **1993**, *97*, 11681.
(25) (a) Krasnoperov, L. N.; Chesnokov, E. N.; Panfilov, V. N. *Chem. Phys. Lett*. **1984**, *89*, 297. (b) Chasovnikov, S. A.; Krasnoperov, L. N. *Khim. Fiz*. **1987**, *6*, 956.
(26) Slagle, I. R.; Bernhardt, J. R.; Gutman, D. *Chem. Phys. Lett*. **1988**, *149*, 180.
(27) Sugawara, K.; Nakanaga, T.; Takeo, H.; Matsumara, C. *Ibid*. **1989**, *157*, 309.
(28) Perry, R. A.; Siebers, D. L. *Nature* **1986**, *324*, 657.
(29) Mertens, J. D.; Kohse-Hoinghaus, K.; Hanson, R. K.; Bowman, C. T. *Int. J. Chem. Kinet*. **1991**, *23*, 655.
(30) Miller, J. A.; Melius, C. F. *Int. J. Chem. Kinet*. **1992**, *24*, 421.
(31) Louge, M. Y.; Hanson, R. K. *Combust. Flame* **1984**, *58*, 291.
(32) Perry, R. A. *J. Chem. Phys*. **1985**, *82*, 5485.
(33) Caldin, E. F. *Chem. Rev*. **1969**, *69*, 135.
(34) Johnston, H. S.; Rapp, D. *J. Am. Chem. Soc*. **1961**, *83*, 1.
(35) (a) Chandra, A. K.; Malar, E. J. P.; Sengupta, D. *Int. J. Quantum Chem*. **1992**, *41*, 351. (b) Chandra, A. K.; Rao, V. S. *Int. J. Quantum Chem.* **1993**, *47*, 437. (c) Pacey, P. D.; Siebrand, W. *Can. J. Chem.* **1988**, *66*, 875.

JP952778Q